PAPER

Check for updates

Laccase-immobilized biochar as a unique host matrix for electrochemical detection of gallic acid: a sustainable engineering approach†

Sona Mariam Thomas, [ID] [a] Rijo Rajeev,[bc] Sariga,[bc] Libina Benny,[bc] Sandra Jose[bc] and Anitha Varghese [ID] *[bc]

An electrochemical platform for the detection of organic persistent polyphenolic pollutant, gallic acid (GA), was fabricated using an enzyme-immobilization approach over acid-functionalized biochar (f-BC) modified carbon fiber electrode (CFP) electrode. The f-BC was synthesized from dried pineapple leaves and was characterised using X-ray diffraction analysis (XRD), Raman spectroscopy, scanning electron microscopy (SEM), Fourier Transform-Infrared Spectroscopy (FT-IR), and X-ray photoelectron spectroscopy (XPS) for analysing the physicochemical characteristics. The SEM image of Lac/f-BC/CFP confirmed the presence of a porous and granulated surface upon laccase immobilization, while the FTIR spectrum confirmed the presence of C=O stretch and N−H bend, indicating amide bond formation. The acid treatment of biochar introduced −OH and −COOH groups that further aided in the successful immobilization of laccase *via* covalent bonding. The fabricated electrode could demonstrate a linear response within the concentration range of 0.012−40 µM and a low detection limit (LOD) of 9 nM with high selectivity. The fabricated electrode also showcased high practical utility as it could attain high recovery percentage during real sample analysis in tap, pond, sewage and industrial effluent samples.

1. Introduction

Gallic acid (3,4,5-trihydroxybenzoic acid) is a dissolved organic persistent polyphenolic pollutant (DOPP) that has deleterious effects on humans, animals, and the environment.[1] DOPPs enter the aquatic environment due to the deterioration or decomposition of naturally occurring organic materials in the water, domestic and industrial waste dumping into water bodies, and runoffs from agricultural regions. GA is a crucial raw material in pharmaceutical, chemical, and food industries that is discharged in a sizeable quantity into its wastewater.[2] This causes increased chemical oxygen demand of water, leading to a change in taste and odour. It also generates by-products such as haloacetic acids and chloroform, which can harm a person's kidney, liver, and other organs.[3] As a result, it is important and necessary to identify and measure the presence of GA in the environment. Contrary to the traditional methods such as mass spectrometry, high-performance liquid chromatography, capillary zone electrophoresis, and

spectrophotometric techniques that demand the need for expensive equipment, large amounts of toxic solvents and complicated operation procedure electrochemical approach with chemically modified electrodes are advantageous.[4,5] Electrochemical sensing is a facile, rapid, robust, and cost-effective strategy. From the literature, various metal oxides, metal nanoparticles, and carbon-based material composites have been employed to determine GA.[6,7]

Over the past few decades, electrochemical sensing of various analytes has garnered significant attention from the community.[8] It has been shown to be an innovative tool for qualitative and quantitative examination of several target substrates across a broad spectrum of applications. Among the various bioreceptor-based biosensors, enzyme-based biosensors are superior as they offer high selectivity and sensitivity, portability, are inexpensive, and have the potential for miniaturisation. Immobilized enzymes could preserve catalytic activity and stability in contrast to mobile enzymes, allowing for ongoing and recurrent use.[9] Covalent immobilization, entrapment, cross-linking, and adsorption are the various approaches for enzyme immobilization. Covalent binding is the most widely used because of its ability to form stable complexes with enzymes and the substrate.[10] The enzyme's thiol, amino, and carboxylic groups are involved in this linkage. Carbonaceous materials support scaffolds efficiently due to their larger active surface area and efficient electron transfer kinetics.[11] The thermal breakdown of biomass in an oxygen-limited environment created biochar (BC), and low-cost mass production

[a]Department of Biotechnology, Manipal Institute of Technology, Manipal Academy of Higher Education, Manipal, Karnataka-576104, India

[b]Department of Chemistry, Christ University, Bangalore, Karnataka-560029, India

[c]Centre for Renewable Energy and Environmental Sustainability, Christ University, Karnataka-560029, India. E-mail: anitha.varghese@christuniversity.in

† Electronic supplementary information (ESI) available. See DOI: https://doi.org/10.1039/d5ra02682b

boosted the applicability of BC in various fields.[12–14] This porous carbon-rich substance is advantageous due to its large-scale availability, cost-effectiveness, highly porous structure, and facile preparation route.[15,16] It is feasible to incorporate organic and inorganic functionalities into this material through functionalization.[17] Functionalized materials have been used extensively in various industries, including food processing, cosmetics, textiles, pharmaceuticals, and electronics.[18] Functionalizing biochar helps to introduce the acid group. As a result, the functional groups in the enzyme and the functional groups on the biochar surface create persistent covalent connections.

Guo *et al.* synthesized SWCNT@MSNs based on single-walled carbon nanotubes (SWCNT) and mesoporous silica nanoparticles (MSNs) for the detection of GA. The presence of both SWCNT and MSNs contributed significantly to the enhanced electrical conductivity, which led to the heightened electroanalytical performance of the developed electrode. The electrode could demonstrate a LOD (3.806 nM) and a linear range (0.03–30 μM). In addition, high, reproducibility, repeatability, and selectivity in the presence of various interferents were displayed by the electrode.[19] Hyder *et al.* proposed an electrode based on the utilization of methods involving covalent treatment and electrostatic self-assembly for grafting calixarene derivatives with hydroxyl groups on graphene oxide surfaces. The reported electrode was capable of detecting ultra-low concentrations of GA with a LOQ and LOD of 0.03 and 0.01 μM. Also, the electrode displayed a wide

linear range of 10–100 μM along with high anti-interference and stability.[20] However, these research works involve cumbersome material preparation that can take significant time and resources. In the present investigation, the support material is derived from naturally derived biomass with further acid functionalization assisting in stable laccase immobilization.

The current work takes the aforementioned advantages of laccase and biochar obtained from dried pineapple leaves. The biochar was later acid functionalized (f-BC) and subsequently immobilized with laccase on the electrode for detection of GA, as shown in Scheme 1. The presence of f-BC acts as a stable support matrix and provides ample surface-active sites for laccase immobilization. This work explores the electrochemical behaviour and kinetic parameters associated with the electrochemical quantification of GA. The fabricated electrode could demonstrate a linear response within the concentration range 0.012–40 μM and a low detection limit (LOD) of 9 nM with high selectivity and sensitivity. The designed electrode also showcased high practical utility in detecting GA in tap, pond, sewage, and industrial water samples with high recovery rates (99.40% to 99.90%).

2. Experimental section

2.1 Chemicals required and instrumentation techniques

Analytical grade hydrochloric acid, nitric acid, sulphuric acid, $K_3[Fe(CN)_6]$, K_2HPO_4, and KH_2PO_4 were obtained from SD Fine
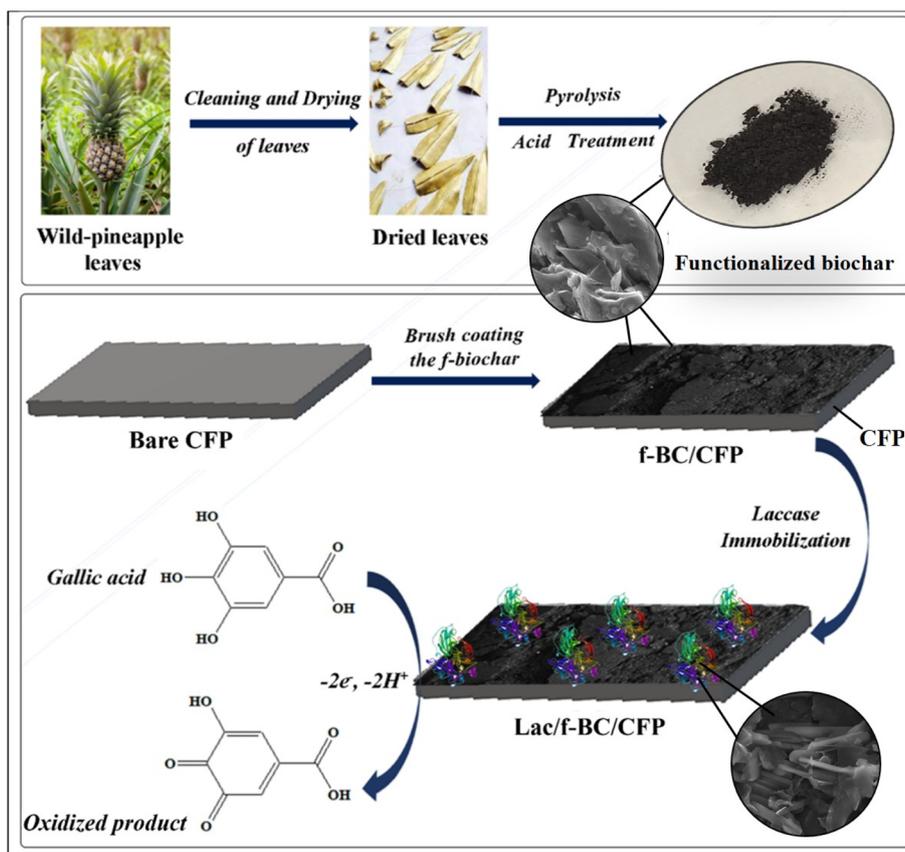
Scheme 1 Preparation of laccase immobilized acid functionalized biochar towards electrochemical detection of GA.

Pvt Ltd, India. Other chemicals such as laccase (source: Trametes versicolor), N-hydroxy succinimide (NHS), and 1-ethyl-3-(30-dimethylaminopropyl)carbodiimide (EDC) were procured from Sigma-Aldrich. A three-electrode-based electrochemical setup consisting of a working electrode, saturated calomel as a reference electrode, and Pt as a counter electrode was used for the investigation. Carbon fiber paper with the dimensions (1 cm × 0.50 cm) was utilized as a substrate for the working electrode (geometrical surface area = 0.70 cm^2). Electrochemical studies were carried out with equimolar concentrations of K_2HPO_4 and KH_2PO_4 to prepare a phosphate buffer solution, $K_3Fe(CN)_6$ (potassium ferricyanide), with a molarity of 5 mM.

CHI electrochemical workstation (model CHI608E) was used to conduct electroanalytical studies. Thermo Nicolet, Avatar 370 was utilized for recording the Fourier transform infrared spectra. Scanning electron microscopy (SEM) analysis of the electrode surface was carried out using a JSM-5600LV microscope (JEOL, Ltd, Japan). X-ray photoelectron spectroscopy results were conducted employing a K-Alpha XPS spectrometer (Thermo Fisher).

2.2 Synthesis of biochar followed by acid functionalization

The wild pineapple leaves were washed and sun-dried. For the removal of the carbon-rich fibers inside the dried leaves, it was further finely chopped. To enhance surface area and porosity, the dried pineapple leaves were activated with 0.1 M KOH solution at 200 °C for 3 days. In addition, the activated carbon fibers were incinerated at 10 °C per minute while raising the temperature from 150 °C to 500 °C using a muffle furnace. The resulting mass was ground, sieved, and autoclaved with steam at 16 lbs for 20 minutes at 120 °C to produce biochar.

The functionalization of biochar via acid treatment was done by taking 1 g of biochar in 80 mL of 5 M H_2SO_4/HNO_3 (3 : 1 v/v) mixture, followed by mixing at 250 rpm at room temperature overnight. The functionalized biochar was washed with milli-Q water several times to remove residual acids and filtered using Whatman filter paper to collect the functionalized BC and further dried at 35 °C. Once the acid functionalization of the BC was achieved, the collected f-BC was then mixed with N-methyl-2-pyrrolidone (NMP) as a solvent and polyvinylidene fluoride (PVDF) powder as a binder. The ratio of f-BC and PVDF was taken as 9 : 1 and was brush-coated onto the CFP electrode using a fine paint brush and kept for drying at room temperature in an incubator.

2.3 Immobilization of laccase onto functionalized biochar

A two-step diimide-activated amidation process achieved the immobilization of laccase on the f-BC/CFP surface. Initially, f-BC/CFP was dipped inside a solution of equimolar amounts of NHS and EDC (pH = 7). This was followed by continuous stirring for 60 min. An unstable reactive amine ester is formed, enabling laccase binding on f-BC/CFP. Following this, the intermediate-activated f-BC/CFP is reacted with a laccase solution (14 mg mL^{-1}) under optimal pH conditions and kept for 120 min. Later, the Lac/f-BC/CFP electrode was washed several times with PBS and stored at 4 °C for durability studies.

2.4 Electrochemical analysis

GA was electrochemically detected using cyclic voltammetry (CV) and differential pulse voltammetry (DPV) methods. Using CV for bare CFP and modified electrode (Lac/f-BC/CFP and f-BC/CFP) in an electrolyte solution containing 0.10 M PBS (pH 7), the electrochemical activity of GA was investigated with a scan rate of 0.05 V s^{-1}. The quantitative determination of GA was inferred by DPV investigations, which involved sweeping fabricated electrode between 0.05–0.80 V.

3. Results and discussion

3.1 Physico-chemical characterisation

The f-BC obtained from the hydrothermal method, followed by acid functionalization, was subjected to various characterization techniques for studying its structural and chemical features. The biochar showcases a porous, fragmented, and irregular surface, which is a characteristic feature of pyrolyzed biomass-derived carbon materials (Fig. 1a). The presence of these pores provides a high surface area for effective surface functionalization. Upon acid treatment, the f-BC (Fig. 1b) exhibits a noticeable change in texture with relatively cleaner and more etched surface, confirming the successful introduction of acidic functional groups. In case of SEM images of laccase, globular and amorphous morphology was observed, which is consistent with the aggregated form of the enzyme (Fig. 1c). Upon immobilisation of laccase on f-BC, the presence of granulated structures embedded on the biochar surface can be observed, substantiating successful enzyme loading on the Lac/f-BC surface, as observed from Fig. 1d. The presence of C, N, and O were predominant in all the samples as shown in the EDS graph (Fig. S1a–d†).

XRD analysis was conducted to confirm the degree of carbon ordering of the synthesized f-BC and a crystalline nature was observed as shown in Fig. 2a. There is a main broad peak in the low angle region (10°–35°) denoted by (002) associated with stacking of the graphitic basal plan and parallel organization of carbonized morphology in biochar. The peak broadening is a result of the minute dimensions of crystallites perpendicular to aromatic layers. In addition, the non-labeled sharp peaks are analogous to the presence of inorganic components with a heterogeneous surface.[21] The f-BC showcases a crystalline structure assigned to the graphitic phase, similar to the already reported literature.[22] Raman spectroscopy was employed to examine the crystal morphology and chemical makeup of the synthesized f-BC (Fig. 2b). From the spectrum, the presence of two peaks at 1361 cm^{-1} and 1586 cm^{-1} correlating to D- and G-bands can be observed.[23] The sp^2-hybridized domain-rich CFP and biochar have π–π interactions between the graphitic planes of the CFP and the conjugated aromatic domains in biochar, which helps in maintaining a stable physical contact of f-biochar with CFP with reduced delamination during electrochemical experiments. The acid treatment of biochar brings in various groups, including –OH and –COOH, which are capable of forming electrostatic interactions of hydrogen bonding with the hydroxyl or carbonyl functional groups available on the
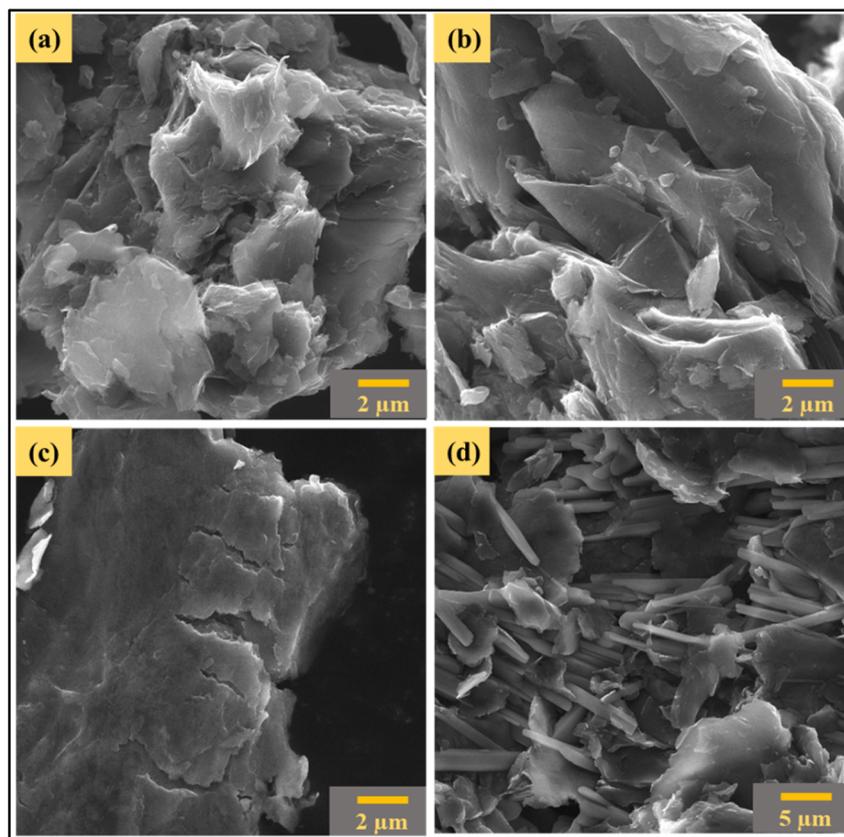
Fig. 1 FESEM image of (a) BC, (b) f-BC, (c) Laccase, and (d) Lac/f-BC/CFP.

slightly oxidised surface of CFP. This leads to an enhancement in the formation of shorter and conductive pathways between f-biochar and CFP. The presence of acid functional groups on the bare CFP electrode helps in the successful immobilization of laccase *via* covalent bonding.

The roughness and thickness of the prepared electrode were characterised using optical profilometry data, as shown in Fig. S2.† The BC/CFP electrode exhibited an average surface roughness (S_a) of 6.53 μm with an average altitudinal profile of 53.40 μm (Fig. S2a†). Upon acid-treatment, the f-BC/CFP displayed a higher S_a of 7.61 μm while the average height reduced to 43 μm (Fig. S2b†). Acid treatment of biochar may cause the removal of impurities, ash, metals, and minerals, and add porosity, enhanced surface area, and terminal functional groups, which leads to a lower particle size with increased roughness. After enzyme immobilization, the Lac/f-BC/CFP showed a S_a of 10.74 μm with an average altitude of 66.10 μm (Fig. S2c†). This increased S_a for Lac/f-BC/CFP represents
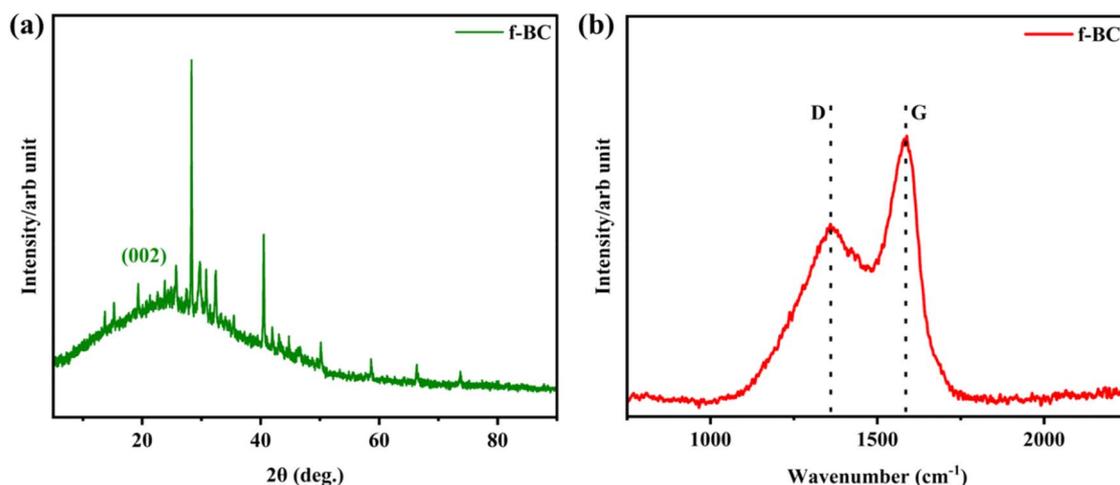

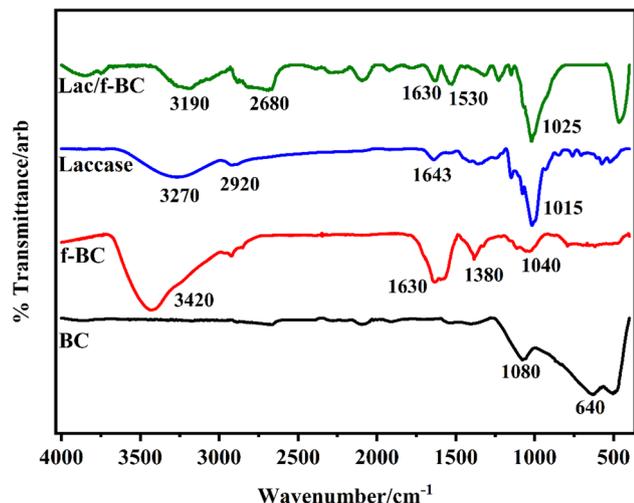Fig. 2 (a) XRD plot and (b) Raman spectrum of f-BC.

Fig. 3 FTIR spectra of BC, f-BC, laccase, and Lac/f-BC.

a higher surface irregularity, leading to an increased exposure of specific reactive sites, which helps foster electrocatalysis at the interface. The surface coverage of f-BC on CFP can be evidenced

from its SEM micrograph and optical profilometry images, which show a consistent carbon mass coating on CFP. Also, coating consistency was maintained across multiple electrode preparations, following the same brush-coating protocol to obtain consistent experimental results.

3.1.1 Evidence for laccase immobilization on f-BC/CFP. FTIR analysis was conducted to confirm the presence of functional groups and the synthesis of all three modifications, as shown in Fig. 3. The biochar displays a broad and weak band near 1080 cm^{-1} owing to the C–O functional groups.[24] The peak at 640 cm^{-1} may be due to C–H bending vibrations resulting from lignin and cellulose in the biochar.[25] The presence of peaks at 1630 and 1380 cm^{-1} confirms the presence of a graphitic core backbone. In addition, the 1040 cm^{-1} peak is due to a C–O–C bond in the carbon framework, substantiating the successful synthesis of f-BC. In the case of laccase, the peak at 3270 cm^{-1} corresponds to the H-bonded with –OH stretch, indicating the existence of a phenyl group.[26] The peak at 2920 cm^{-1} confirmed the presence of asymmetric C–H stretching.[27] The 1643 cm^{-1} peak is associated with the presence of the carbonyl group (C=O), and the peak at 1015 cm^{-1} belongs to the aliphatic amine (C–N).[28] Successful laccase
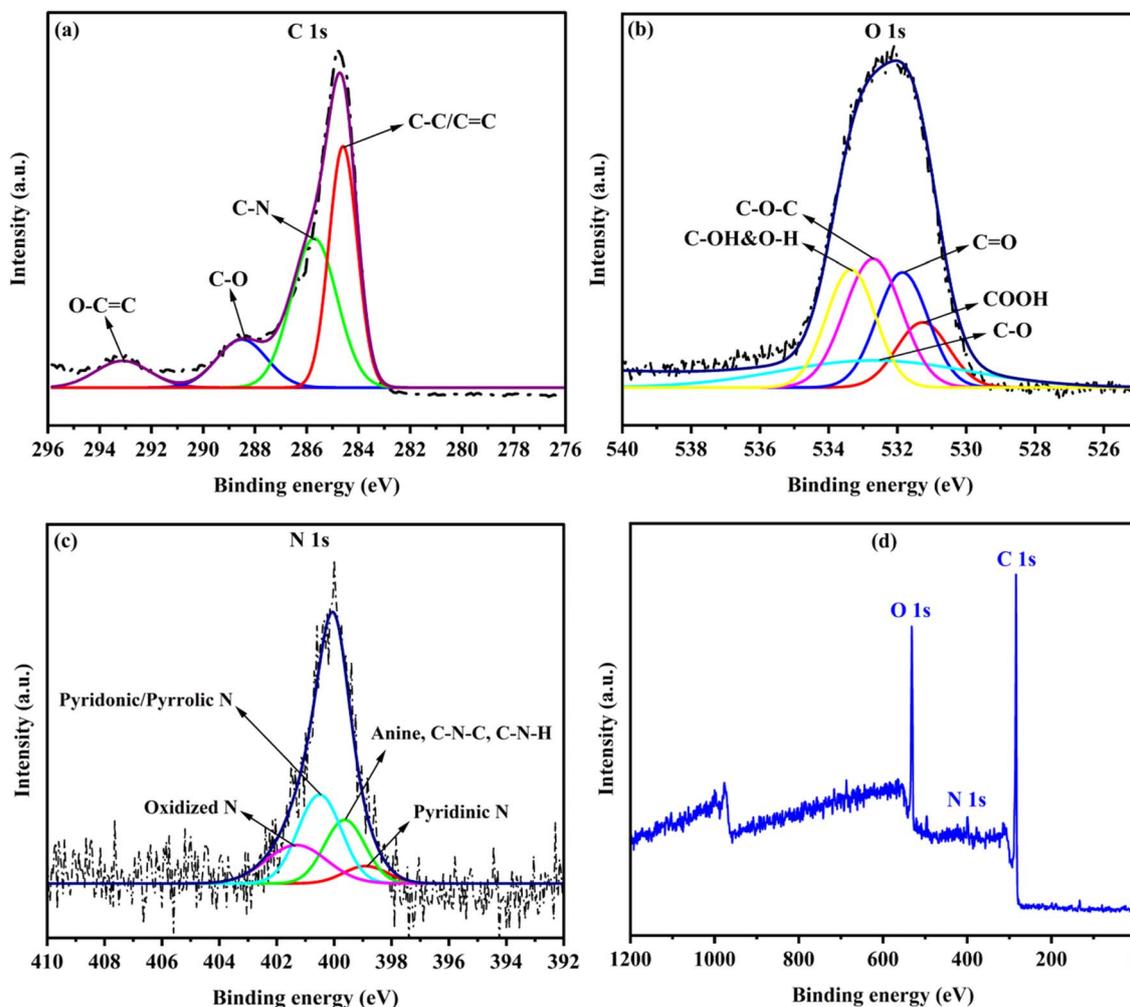

Fig. 4 XPS analysis of Lac/f-BC/CFP. Deconvoluted XPS plots in the (a) C 1s, (b) O 1s, (c) N 1s, and (d) XPS survey spectrum.

immobilization on the f-BC could be substantiated using the 1630 and 1530 cm^{-1} peaks that agree with both C=O stretch and N–H bend, indicating amide bond formation.[29]

XPS analysis was performed to understand the chemical makeup and functional groups present in the Lac/f-BC. The survey scan revealed the presence of C, O, and N in the Lac/f-BC/CFP as shown in Fig. 4. Upon deconvolution, the C 1s spectrum gave rise to four peaks in total. Among these, peaks at 284.42 are analogous to the graphitic C–C bond.[30] A peak confirmed the successful laccase immobilization at 285.51 eV, which corresponds to the amide bond of laccase.[31] The peaks at 288.40 and 293.00 eV are due to the C=O bond and O–C=C groups.[32] In the case of the O 1s spectrum, the photoelectron peaks were observed at 531.22, 531.80, 532.54, 532.82, and 533.51 eV corresponding to COOH, C=O, C–O, C–O–C, and C–OH groups.[33,34] The deconvolution of N 1s resulted in four peaks at 398.41, 399.53, 400.50, and 402.31 eV correlating to the pyridinic N, amine C–N–C, C–N–H, pyridonic/pyrrolic N, and oxidized N respectively.[30]

3.2 Electrochemical studies

3.2.1 Electrochemical properties of developed electrodes.
The electrochemical properties of the developed electrodes were studied by subjecting the electrodes to CV runs in the presence of 0.1 M KCl and 5 mM $[Fe(CN)_6]^{3-/4-}$. Upon analysis, it was understood that all three electrodes showcase a redox couple arising as a result of the redox reaction of $[Fe(CN)_6]^{3-/4-}$ (Fig. 5a). This comes under the category of reversible one-electron redox process, wherein the $[Fe(CN)_6]^{3-}$ (ferricyanide) is in the oxidised form and $[Fe(CN)_6]^{4-}$ (ferrocyanide) is present in reduced form. The observed cathodic peak is due to the reduction of ferricyanide, and the anodic peak corresponds to the oxidation of ferrocyanide. The highest electrocatalytic performance was showcased by f-BC/CFP compared to both Lac/f-BC/CFP and bare CFP electrodes. The presence of the laccase enzyme reduced the electrocatalytic activity of the Lac/f-BC/CFP, substantiating the successful immobilization of laccase.

Electrochemical impedance spectroscopy (EIS) provides information on the impedance changes on the bare and modified CFP electrode surfaces. The Nyquist plots were recorded and utilized for determining the transference of electrons (Fig. 5b). The EIS measurements were conducted for all the fabricated electrodes using 5 mM $[Fe(CN)_6]^{3-/4-}$ as the redox mediator and 0.1 M KCl as electrolyte. The bare CFP displayed an R_{ct} value of 1210 Ω, showcasing low electrical conductivity. Upon fabrication using f-BC, there was a noteworthy reduction in the R_{ct} value (50 Ω). This was attributed to the presence of several sp^2-hybridised carbon atoms as a result of carbonization and the resulting formation of biochar. This, along with the conjugated aromatic structure, helped in the delocalisation of π electrons, thereby resulting in increased electrical conductivity. Also, the extent of pyrolysis leads to the formation of a hierarchical porous structure that, in turn, provides shorter diffusion pathways, higher surface area, and generates several active sites, all of which increase the electrical conductivity. This leads to a significant reduction in R_{ct} for f-BC/CFP.[35,36] The Lac/f-BC/CFP demonstrated an R_{ct} value of 93 Ω. The increased R_{ct} value upon laccase immobilization substantiates successful immobilization on the f-BC/CFP electrode.[37] The observed decrease in the current value is due to the existence of protein molecules that are non-conductive, thereby limiting and reducing the number of channels available for effective electron transference. However, the limited electron transference does not majorly affect the overall electrical performance of the developed electrode, as it shows high selectivity towards the oxidation of GA. The presence of a mediator would have led to a rapid and increased increase in electrical conductivity during analysis of electrocatalytic activity. However, since no mediator was being used, the presence of laccase enzyme hindered the electron transference; thereby, the mentioned electron transference in this case is occurring *via* a direct electron transfer pathway.

3.2.2 Electrochemical performance of fabricated electrodes towards GA detection.
The electrochemical quantification performance of the bare and the modified electrodes for GA detection (20 μM) was analysed at 0.05 V s^{-1} in 0.20 M PBS (pH 6.50). The GA electrooxidation pathway is demonstrated in Fig. 6a. Fig. 6b shows the CV curves for oxidation of 20 μM GA at bare, BC/CFP, f-BC/CFP, and Lac/f-BC/CFP electrodes. The oxidation peak observed during the electrochemical oxidation
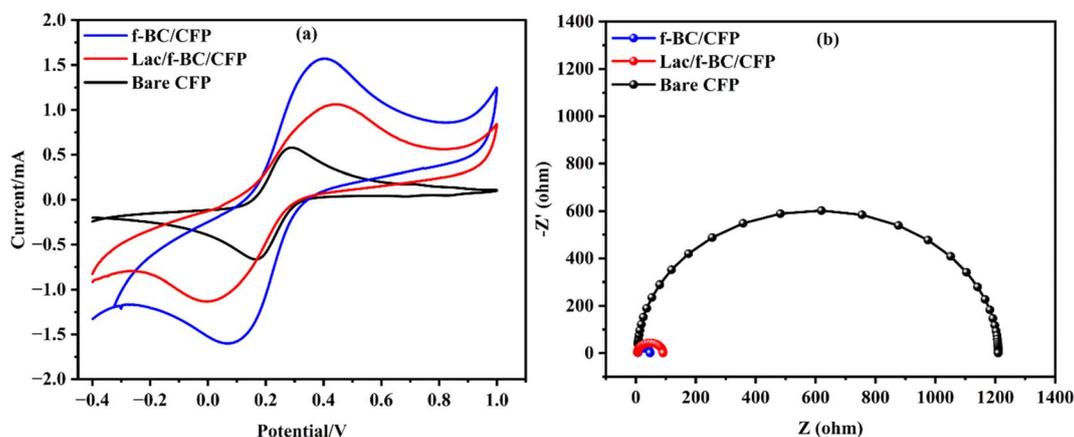

Fig. 5 (a) CV curves and (b) Nyquist plots of bare and modified electrodes in 5 mM redox mediator and 0.10 M KCl solution.

of gallic acid is due to the oxidation of the catechol moiety (*ortho*-dihydroxyl groups), forming an *ortho*-quinone. This oxidation process involves the loss of two protons and two electrons, resulting in a clear anodic (oxidation) peak. Since the bare CFP was not fabricated with any modification, it showed the least electrochemical conductivity, thereby exhibiting weak current response (4.41×10^{-6} A cm^{-2}) at 0.65 V. Upon modifying with BC, the resultant BC/CFP showed an increase in the current response (5.72×10^{-6} A cm^{-2}) at 0.63 V due to enhanced surface area and conductivity. f-BC/CFP could display a much more intense oxidation current response at 0.61 V with a corresponding current value at 8.03×10^{-6} A cm^{-2} for GA because of a heightened number of surface-active sites, resulting in enhanced electrical conductivity. Among all the modified electrodes, the highest oxidation response (1.89×10^{-5} A cm^{-2}) at 0.63 V was observed in the case of the Lac/f-BC/CFP electrode. The presence of various factors, such as enhanced surface area and porous structure of the f-BC, leads to the generation of

abundant surface-active sites for effective immobilization of the laccase enzyme. Moreover, the inclusion of laccase immobilization led to the ameliorated enzyme loading and improved covalent bonding, resulting in effective oxidation of GA at the Lac/f-BC/CFP electrode.

3.3 Influence of pH on GA detection

Studying the effect of pH is crucial for determining the involvement of protons and electrons in a given electro-oxidation reaction mechanism. Electrochemical detection of GA (20 μM) using Lac/f-BC/CFP electrode was analyzed in the presence of 0.10 M PBS using different pH solutions (pH = 5.00–8.00). Upon recording of the CV, it was observed that there was an enhancement in the GA oxidation current from pH 5.00–7.00, and later there was a reduction in the current peak from pH 7.00–8.00. The reason for an increase and decrease in the GA oxidation peak was attributed to the deprotonation taking place when shifting to higher pH values. This ultimately results in diminished current signals, leading to a reduction in the GA oxidation current. Considering that pH 7 displayed the most intense oxidation current peak, it was chosen to complete all the experimental electrochemical procedures.

The relation between pH against E_{pa} (Fig. S3†) has been described in Nernstian eqn (2)

$$E_p = -0.06\ \text{pH} + 0.95\ (R^2 = 0.99) \tag{1}$$

$$E_p = 0.0592\ m/n\ \text{pH} + b \tag{2}$$

As the value of the slope is closely similar to 0.0592, engagement of equal no. of e$^-$ and H$^+$ is observed. E_p = peak potential, m = number of H$^+$, n = number of e$^-$, and b = intercept.

3.4 Mechanism of GA electro-oxidation reaction at Lac/f-BC/CFP

Different CV curves were recorded in the range of 0.01–0.10 V s^{-1} to substantiate the reaction mechanism for GA detection at
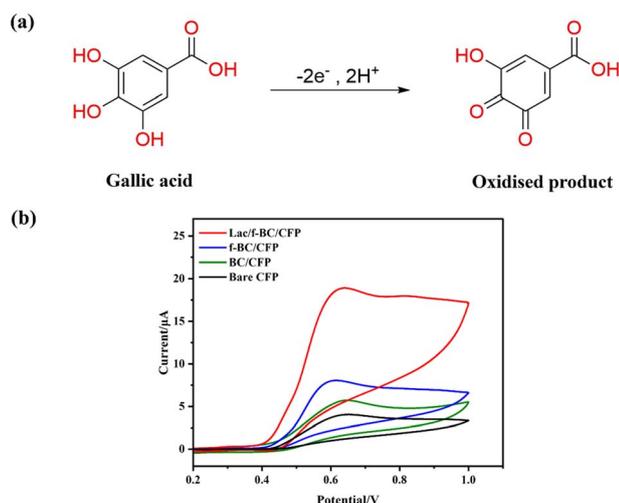

Fig. 6 (a) Electro-oxidation pathway of GA, (b) CV curves for oxidation of 20 μM GA at bare, BC/CFP, f-BC/CFP, and Lac/f-BC/CFP electrode.
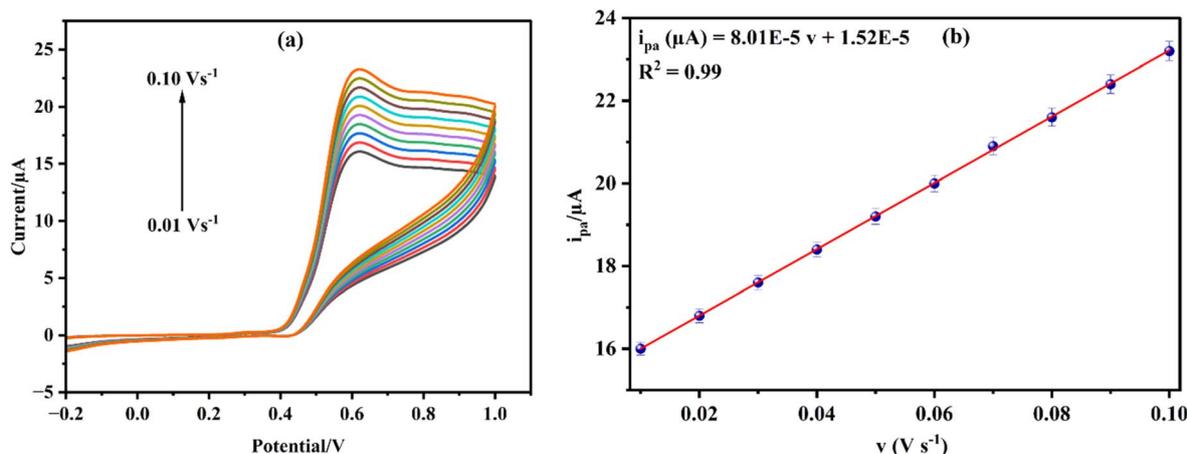

Fig. 7 (a) CV curves of 20 μM GA at Lac/f-BC/CFP electrode in the presence of different scan rates. (b) Linear relation between anodic current signals and differing scan rates.
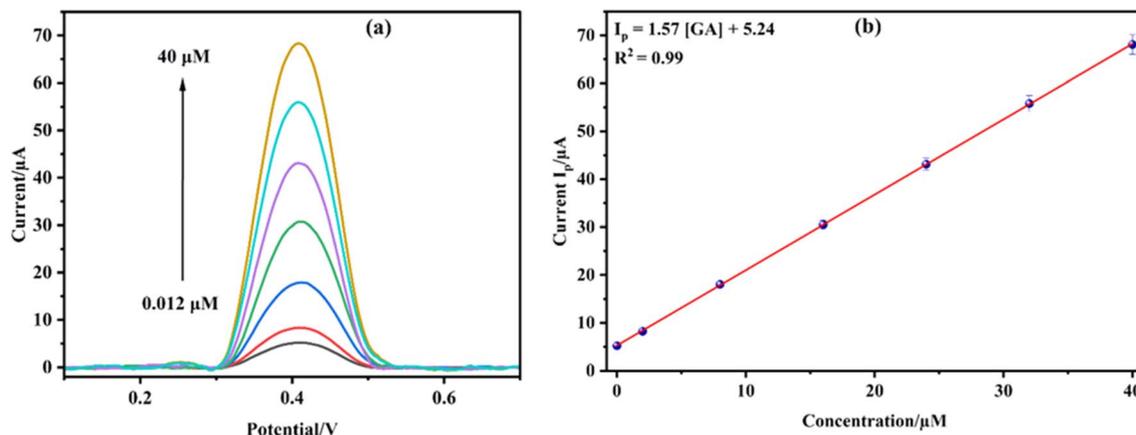
Fig. 8 (a) DPV analysis of Lac/f–BC/CFP electrode with various concentrations of GA (b) calibration plot of GA employing Lac/f–BC/CFP electrode.

the Lac/f-BC/CFP electrode (Fig. 7a). It was observed that the anodic current signals were linearly increased with differing scan rates. The attainment of a linear correlation along with R^2 = 0.99 confirms that the GA electro-oxidation occurs *via* an adsorption-mediated mechanism (Fig. 7b).[38]

The number of electrons involved in the case of GA electro-oxidation was found to be 2.03 (equivalent to 2) using eqn (3):

$$E_p - E_{p/2} = 0.0592/n \qquad (3)$$

In eqn (3), E_p = peak potential and $E_{p/2}$ = half peak potential.

3.5 Analytical performance of Lac/f-BC/CFP electrodes towards GA electro-oxidation

The analytical performance of the fabricated Lac/f-BC/CFP electrode towards GA electro-oxidation was studied by employing the DPV technique under optimized conditions, as shown in Fig. 8a. Compared to the CV technique, DPV is considered to be more effective as it showcases higher selectivity, less background current noise, and better sensitivity. The attainment of a linear graph confirmed the enhanced sensitivity of the Lac/f-BC/CFP electrode upon plotting the oxidation current against the increasing GA concentration.

Table 1 Comparison of different electrodes with Lac/f-BC/CFP towards electrochemical quantification of GA. The table also includes comparative data for carbon-based electrodes for the detection of other environmental pollutants

| Electrodes	Analyte	Fabrication method	Linear range (μM)	LOD (μM)	Sensitivity	Stability	Ref.
SiO₂ nano/CPE	Gallic acid	Hand-mixing of graphite powder with paraffin oil	0.8–100	0.25	1790.7 (μA mM⁻¹)	8 weeks	39
TiO₂ nanoparticle-modified electrode	Gallic acid	Hand-mixing of graphite powder with paraffin oil	2.5–150	0.94	999.4 A mM⁻¹	—	40
MIP/TiO₂@CNTs/GCE	Gallic acid	Electropolymerization of MIP film	50–700	0.012	0.02 μA μM⁻¹	—	41
Ni-MOF/PEDOT-2/GCE	Gallic acid	Ultrasonic treatment	0.8–25.5	0.559	—	—	42
NPGA-GCE DPV	Gallic acid	Modified Hummers' method + drop-casting on GCE	2.5–1000	0.067	—	21 days	43
AuCMs/SF-GR/GCE	Gallic acid	Modified Hummers' method + drop-casting on GCE	0.05–8.0	0.0107	—	15 days	44
3D IPCNT/CNS/GCE	Gallic acid	Ball-milling + thermal decomposition + drop casting	0.05–20	0.016	—	—	45
SPCB@MSNs/GCE	Gallic acid	Ultrasonic-assisted strategy + drop casting	0.5–10	0.004911	—	—	46
CME/GC/CSs/AC-CNTs	Gallic acid	Chemical vapor deposition	0–5360	3.64	—	10 days	47
Co-Pi/PTAA/CFP	Metol	Electropolymerization	0.006–0.8	0.002	—	20 days	48
Lac/PAA/CFP	*p*-nonylphenol	Electropolymerization + laccase immobilization	0.005–0.25	0.00174	—	20 days	49
Cu-BTC-MOF/PTA/CFP	Resorcinol	Electrodeposition + electropolymerization	0.02–350	0.008	—	3 weeks	50
Lac/f-BC/CFP electrode	Gallic acid	Carbonization + laccase immobilization	0.012–40	0.009	1.57 μA μM⁻¹	5 weeks	Present work
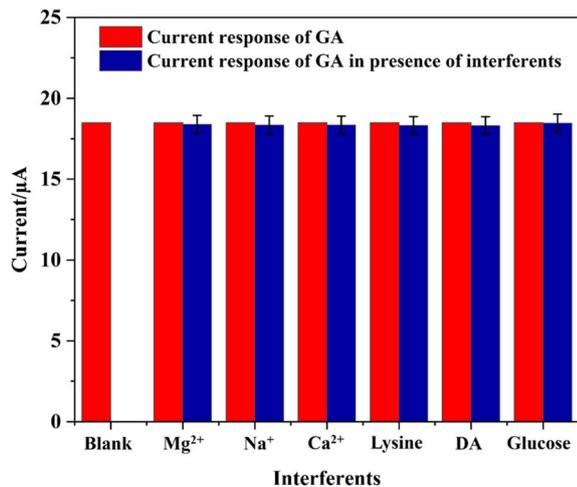
Fig. 9 Plot of the current activity of Lac/f-BC/CFP electrode in GA (20 μM) in the presence of different interfering species.

The obtained calibration curve is mentioned in (Fig. 8b) and is interpreted in eqn (4):

$$I_p(A) = 1.57 [GA] + 5.24 (R^2 = 0.99) \qquad (4)$$

The formula for LOD = 3.3 σ/S and LOQ = 10 σ/S gave 9 nM and 27.29 nM values, respectively. The linear window for the Lac/f-BC/CFP electrode was found to be 0.012–40 μM, along with a sensitivity of 1.57 μA μM^{-1}. When compared with the already reported literature in terms of analytical performance, the devised electrode's analytical performance, as mentioned in Table 1, demonstrates the effectiveness of the fabricated electrode.

3.6 Interference studies

Studying the interference property is an extremely important factor for evaluating the electrochemical sensing performance of the devised electrode. Fig. 9 shows the DPV measurement results of GA detection (20 μM) using the Lac/f-BC/CFP

electrode in the presence of different interfering species, including Mg^{2+}, Na$^+$, Ca^{2+}, lysine, dopamine, and glucose. Adding higher concentrations of these interfering species (200 μM) resulted in no variation in the current and potential of GA detection. Therefore, the Lac/f-BC/CFP electrode demonstrates satisfactory selectivity towards GA quantification.

3.7 Analytical applicability of Lac/f-BC/CFP electrode

In order to validate the applicability of the Lac/f-BC/CFP electrode towards GA detection, spiked samples of tap, pond, sewage, and industrial water were used as real samples (Table 2). The methodology adopted was highly suitable and effective in the accurate determination of GA concentration in both samples, providing valuable insights into the quality of the tested samples. The average recovery rate was noticed between 99.40% and 99.90% with a low RSD value, therefore substantiating real-world applicability for Lac/f-BC/CFP electrode. The matrix effect relates to potential interference from co-existing constituents in complex real-world samples such as organic and inorganic ions. The matrix effect was investigated by performing the spike recovery experiment wherein known concentrations of GA were added to the real water samples (tap water, pond water, sewage water, and industrial effluent), and their recovery values were compared with standard values. Since high recovery rates (99.40% to 99.90%) were obtained with low RSD values, indicating that the electrode response has minimal interference from matrix components. Therefore, Lac/f-BC/CFP electrode showcased excellent selectivity and sensitivity in the presence of possible interferents, substantiating the practical utility in environmental monitoring of GA.

3.8 Reproducibility, repeatability, and stability studies of Lac/f-BC/CFP

The reproducibility, repeatability, and durability are the most important characteristics of a fabricated electrode as they have an overall effect on their utilization capabilities. Reproducibility studies for the Lac/f-BC/CFP electrode were conducted by recording CV curve results from the five electrodes of the same

Table 2 Quantification of GA levels in tap, pond, sewage and industrial water employing Lac/f-BC/CFP electrode

Sample	Concentration (added) (μM)	Concentration (observed) (μM)	Recovery (%)	RSD[a] (%)
Tap water (A)	3.00	2.99	99.9	0.99
	6.00	8.96	99.6	0.97
	9.00	17.95	99.4	0.95
Pond water (B)	3.00	2.97	99.7	0.95
	6.00	8.98	99.8	0.96
	9.00	17.99	99.9	0.98
Sewage water (C)	3.00	2.98	99.6	0.95
	6.00	8.99	99.9	0.98
	9.00	17.98	99.8	0.97
Industrial effluent (D)	3.00	2.95	99.5	0.94
	6.00	8.98	99.4	0.92
	9.00	17.97	99.6	0.95

[a] Mean value of 3 determinations.

modification. The high reproducibility of the proposed electrode towards GA (20 μM) quantification was confirmed on acquisition of 1.11% RSD (Fig. S4a†). An excellent repeatability was also noticed in the case of GA detection by Lac/f-BC/CFP electrode for 10 CV recordings, as they could achieve high throughput with minimal RSD values (1.14%) as displayed in Fig. S4b.† The durability studies for the Lac/f-BC/CFP electrode were conducted by recording CV responses for a total period of 5 weeks. These recordings were done on the particular day of each week under optimal conditions. The fabricated electrodes were stored in cold conditions (5 °C) between the specific recording dates. It was observed that the electrodes could retain up to 95% of their oxidation current response and demonstrate no significant changes in the current and potential values towards GA quantification (Fig. S4c†).

4. Conclusion

This work reports the development of a facile and ultrasensitive electrode for the detection of GA. The fabricated electrode is based on laccase immobilized on an acid-functionalized biochar based on dried pineapple leaves. The f-BC acts as an ideal support matrix by providing abundant surface-active sites and a porous framework for effective laccase immobilization. Furthermore, immobilization of laccase on f-BC leads to improved selectivity in Lac/f-BC/CFP electrode, ameliorating the electrocatalytic oxidation of GA. The designed electrode showcased an LOD of 9 nM and a linear window of 0.012–40 μM. The proposed electrode demonstrates superior interference-free quantification, stability, and reproducibility towards electrochemical GA detection. The real sample detection ability, when tested on tap, pond, sewage, and industrial water samples, could demonstrate a 99.40–99.90% recovery, showcasing excellent practical applicability in the detection of GA. The current existing deficiency is the lack of practical applicability of the devised electrode in terms of designing a portable and tabletop device. This can be overcome by fabricating a handheld sensor that would make bench-to-market technology a reality. Also, integrating MIP technology could help in ensuring higher selectivity to ensure the design of cutting-edge sensors. In addition, since the electrode has a batch-mode operation, future work can explore the possibility of real-time continuous monitoring by integration of a microfluidic-based system coupled with artificial intelligence and machine learning.

Data availability

All data supporting the findings of this study are available within the article.

Author contributions

Sona Mariam Thomas: conceptualization, methodology, formal analysis, investigation, writing – original draft; Rijo Rajeev: methodology, formal analysis, writing – original draft; Sariga: methodology, investigation, editing – original draft; Libina Benny: investigation, writing – original draft; Sandra Jose:

formal analysis, writing – original draft; Anitha Varghese: conceptualization, investigation, supervision, writing – review & editing.

Conflicts of interest

The authors declare that they have no known competing financial interests or personal relationships that could have appeared to influence the work reported in this paper.

Acknowledgements

References

1 P. Sivasakthi, H. Amir, S. Sornambikai, N. Ponpandian and C. Viswanathan, *Sens. Actuators, A*, 2020, **315**, 112368.

2 H. Amir, D. Murugesan, N. Ponpandian and C. Viswanathan, *Appl. Phys. A:Mater. Sci. Process.*, 2021, **127**, 1–9.

3 R. M. Rodrigues, D. A. Thadathil, K. Ponmudi, A. George and A. Varghese, *ChemistrySelect*, 2022, **7**, e202200081.

4 H. Franquet-Griell, A. Checa, O. Núñez, J. Saurina, S. Hernández-Cassou and L. Puignou, *J. Agric. Food Chem.*, 2012, **60**, 8340–8349.

5 L. Jaitz, K. Siegl, R. Eder, G. Rak, L. Abranko, G. Koellensperger and S. Hann, *Food Chem.*, 2010, **122**, 366–372.

6 K. Suresh Babu, A. Padmanaban and V. Narayanan, *Inorg. Chem. Commun.*, 2022, **139**, 109400.

7 F. Gao, D. Zheng, H. Tanaka, F. Zhan, X. Yuan, F. Gao and Q. Wang, *Mater. Sci. Eng. C*, 2015, **57**, 279–287.

8 R. Rajeev, A. R. Cherian, D. A. Thadathil and A. Varghese, *Mater. Res. Bull.*, 2024, **169**, 112523.

9 H. H. Nguyen, S. H. Lee, U. J. Lee, C. D. Fermin and M. Kim, *Materials*, 2019, **12**, 121.

10 A. Kumari, R. Rajeev, L. Benny, Y. N. Sudhakar, A. Varghese and G. Hegde, *Adv. Colloid Interface Sci.*, 2021, **297**, 102542.

11 A. M. B. Sariga, S. Kumar, R. Rajeev, D. A. Thadathil and A. Varghese, *Adv. Mater. Interfaces*, 2023, **10**, 2202139.

12 J. Liu, J. Jiang, Y. Meng, A. Aihemaiti, Y. Xu, H. Xiang, Y. Gao and X. Chen, *J. Hazard. Mater.*, 2020, **388**, 122026.

13 P. R. Oliveira, A. C. Lamy-Mendes, E. I. P. Rezende, A. S. Mangrich, L. H. Marcolino Junior and M. F. Bergamini, *Food Chem.*, 2015, **171**, 426–431.

14 G. Singh, K. S. Lakhi, S. Sil, S. V. Bhosale, I. Y. Kim, K. Albahily and A. Vinu, *Carbon*, 2019, **148**, 164–186.

15 Z. Wan, Y. Sun, D. C. W. Tsang, D. Hou, X. Cao, S. Zhang, B. Gao and Y. S. Ok, *Green Chem.*, 2020, **22**, 2688–2711.

16 G. Bijoy, R. Rajeev, L. Benny, S. Jose and A. Varghese, *Chemosphere*, 2022, **307**, 135759.

17 M. K. A. K. Sariga, L. Benny and A. Varghese, *Dyes Pigm.*, 2023, **210**, 111048.

18 J. Jiao, J. Cao, Y. Xia and L. Zhao, *Chem. Eng. J.*, 2016, **306**, 9–16.

19 M. Guo, J. Han, Q. Ran, M. Zhao, Y. Liu, G. Zhu, Z. Wang and H. Zhao, *Ceram. Int.*, 2023, **49**, 37549–37560.

20 A. Hyder, J. A. Buledi, R. Memon, A. Qureshi, J. H. Niazi, A. R. Solangi, S. Memon, A. A. Memon and K. H. Thebo, *Diam. Relat. Mater.*, 2023, **139**, 110357.

21 Y. Liu, X. Zhao, J. Li, D. Ma and R. Han, *Desalination Water Treat.*, 2012, **46**, 115–123.

22 L. F. Morales, K. Herrera, J. E. López and J. F. Saldarriaga, *Heliyon*, 2021, **7**, e08423.

23 Y. Yan, S. Manickam, E. Lester, T. Wu and C. H. Pang, *Ultrason. Sonochem.*, 2021, **73**, 105519.

24 R. Saikia, R. S. Chutia, R. Kataki and K. K. Pant, *Bioresour. Technol.*, 2015, **188**, 265–272.

25 I. Y. Mohammed, Y. A. Abakr, F. K. Kazi, S. Yusup, I. Alshareef and S. A. Chin, *Energies*, 2015, **8**, 3403–3417.

26 A. I. El-Batal, N. M. Elkenawy, A. S. Yassin and M. A. Amin, *Biotechnol. Rep.*, 2015, **5**, 31–39.

27 L. Benny, A. R. Cherian, K. Ponmudi, A. Varghese and G. Hegde, *J. Sci.: Adv. Mater. Devices*, 2022, **7**, 100510.

28 R. Lakshmanan and U. Ramasamy, *Biomass Convers. Biorefin.*, 2022, **13**(16), 14803–14819.

29 L. Benny, A. R. Cherian, A. Varghese, N. Sangwan, P. K. Avti and G. Hegde, *Mol. Catal.*, 2021, **516**, 111999.

30 M. González-Hourcade, G. Simões dos Reis, A. Grimm, V. M. Dinh, E. C. Lima, S. H. Larsson and F. G. Gentili, *J. Cleaner Prod.*, 2022, **348**, 131280.

31 D. A. Thadathil, A. Varghese, C. V. S. Ahamed, K. A. Krishnakumar, S. S. Varma, R. S. Lankalapalli and K. V. Radhakrishnan, *Mol. Catal.*, 2022, **524**, 112314.

32 S. Ge, S. Wang, W. Mai, K. Zhang, M. Tanveer, L. Wang and C. Tian, *Environ. Sci. Pollut. Res.*, 2023, **30**, 66113–66124.

33 S. Ge, S. Wang, W. Mai, K. Zhang, M. Tanveer, L. Wang and C. Tian, *Environ. Sci. Pollut. Res.*, 2023, **30**, 66113–66124.

34 G. Simões Dos Reis, C. Mayandi Subramaniyam, A. D. Cárdenas, S. H. Larsson, M. Thyrel, U. Lassi and F. García-Alvarado, *ACS Omega*, 2022, **7**, 42570–42581.

35 M. Bartoli, M. Troiano, P. Giudicianni, D. Amato, M. Giorcelli, R. Solimene and A. Tagliaferro, *Appl. Energy Combust. Sci.*, 2022, **12**, 100089.

36 H. Huang, R. Qiu, H. Yang, X. Wu, Y. Chen, W. Cao, Q. Yu, J. Zou, G. Peng, F. Gao, Y. Gao, G. Fan, S. Chen and L. Lu, *Nanotechnology*, 2022, **33**, 445501.

37 C. Lou, T. Jing, J. Zhou, J. Tian, Y. Zheng, C. Wang, Z. Zhao, J. Lin, H. Liu, C. Zhao and Z. Guo, *Int. J. Biol. Macromol.*, 2020, **149**, 1130–1138.

38 A. R. Cherian, L. Benny, A. George, U. Sirimahachai, A. Varghese and G. Hegde, *Electrochim. Acta*, 2022, **408**, 139963.

39 J. Tashkhourian and S. F. Nami-Ana, *Mater. Sci. Eng. C*, 2015, **52**, 103–110.

40 J. Tashkhourian, S. F. N. Ana, S. Hashemnia and M. R. Hormozi-Nezhad, *J. Solid State Electrochem.*, 2013, **17**, 157–165.

41 F. Qin, T. Hu, L. You, W. Chen, D. Jia, N. Hu and W. Qi, *Int. J. Electrochem. Sci.*, 2022, **17**, 220426.

42 S. Song, X. Shang, J. Zhao, X. Hu, K. Koh, K. Wang and H. Chen, *Sens. Actuators, B*, 2018, **267**, 357–365.

43 N. Al-Ansi, A. Salah, M. Bawa, S. Adlat, I. Yasmin, A. Abdallah and B. Qi, *Microchem. J.*, 2020, **155**, 104706.

44 Z. Liang, H. Zhai, Z. Chen, H. Wang, S. Wang, Q. Zhou and X. Huang, *Sens. Actuators, B*, 2016, **224**, 915–925.

45 H. Zhao, Q. Ran, Y. Li, B. Li, B. Liu, H. Ma, M. Zhang and S. Komarneni, *J. Mater. Res. Technol.*, 2020, **9**, 9422–9433.

46 H. Zhao, M. Guo, F. Li, Y. Zhou, G. Zhu, Y. Liu, Q. Ran, F. Nie and V. Dubovyk, *J. Mater. Res. Technol.*, 2023, **24**, 2100–2112.

47 A. Terbouche, S. Boulahia, S. Mecerli, C. Ait-Ramdane-Terbouche, H. Belkhalfa, D. Guerniche, M. Sehailia, K. Bachari, D. Mezaoui and D. Hauchard, *Measurement*, 2022, **187**, 110369.

48 S. Jose, A. George, A. R. Cherian and A. Varghese, *Surf. Interfaces*, 2022, **35**, 102416.

49 S. Jose, D. A. Thadathil, M. Ghosh and A. Varghese, *Electrochim. Acta*, 2023, **460**, 142591.

50 S. Jose, M. Ghosh and A. Varghese, *Mater. Adv.*, 2024, **5**, 3812–3823.